Available online at www.sciencedirect.com
ScienceDirect
International Journal of Heat and Mass Transfer 51 (2008) 2123–2138
International Journal of HEAT and MASS TRANSFER
www.elsevier.com/locate/ijhmt

Estimation of heat-transfer characteristics on a fin under wet conditions

Han-Taw Chen *, Hung-Chih Wang

Department of Mechanical Engineering, National Cheng Kung University, Tainan 701, Taiwan

Received 4 May 2007; received in revised form 3 November 2007
Available online 4 January 2008

Abstract

The finite difference method in conjunction with the least-squares scheme and experimental temperature data is proposed to solve the one-dimensional (1-D) and two-dimensional (2-D) inverse heat conduction problems in order to predict the average overall heat-transfer coefficient $\bar{h}$ on a fin and wet fin efficiency η_f for various air speeds under wet conditions. The sensitive and overall heat-transfer coefficients on the fin, the Lewis number and the functional form between the relative humidity and fin temperature are unknown a priori in the present study. In addition, the sensitive and overall heat-transfer coefficients on the fin are also assumed to be non-uniform. Thus the whole fin is divided into several sub-fin regions in order to predict the $\bar{h}$ and η_f values. Variations of these two predicted values with the relative humidity (RH) for various air speeds can be obtained using the present inverse scheme in conjunction with measured fin temperatures. In order to validate the accuracy and reliability of the present inverse scheme, a comparison between the present estimates obtained from the 1-D and 2-D models and exact values is made using simulated temperature data. The results show that the present estimates of the $\bar{h}$ value obtained from the 1-D and 2-D models agree well with the exact values even for the case with the measurement errors. Variations of the $\bar{h}$ and η_f values obtained from 2-D model with the RH value are similar to those obtained from 1-D model for various air speeds. However, the present estimates of the $\bar{h}$ and η_f values obtained from the 2-D model an slightly deviate from those obtained from the 1-D model. It is worth mentioning that the deviation between the $\bar{h}$ value in the downstream region and that in the upstream region can be observed using the 2-D model. This phenomenon cannot be obtained from the 1-D model.

1. Introduction

Finned tube heat exchangers are commonly used in air conditioning. In designing such heat exchangers, it is necessary to consider the interactions between the local heat transfer and flow distribution within the fins. Thus a good estimation of the steady-state heat-transfer characteristics is difficult to be determined using the commercially software, such as STAR CD and FLUENT, etc. However, most of the previous works about the heat-transfer characteristics of the finned tube heat exchangers were limited to the experiments. The fins are always used for the enhancement of heat transfer in the industrial heat exchangers such as dehumidification and air-cooling, etc. This implies that the two-phase flow on the fin can be observed for these industrial heat exchangers. Such problems can be regarded as heat and mass transfer processes because the warm and humid air encounters the cold fin that its temperature can be below the dew point temperature. Thus the actual heat transfer of such problems must include the sensitive heat transfer and latent heat transfer originated by mass transfer. On the other hand, the overall heat-transfer coefficient mainly involves the sensitive heat-transfer coefficient and that due to mass transfer. This also implies that the fin performance of such problems is significantly influenced by the combined heat and mass transfers associated with the cooling and dehumidification of the air. During the dehumidification process, the droplets can drain off the fin surface due to gravity and the forced air flow. With regard to the fin temperature and dew point temperature of the surrounding air, three different states on a fin surface can be observed [1,2]. The fin surface will be completely wet if

* Corresponding author.
E-mail address: htchen@mail.ncku.edu.tw (H.-T. Chen).

0017-9310/$ - see front matter © 2007 Elsevier Ltd. All rights reserved.
doi:10.1016/j.ijheatmasstransfer.2007.11.011

Nomenclature

A_f	lateral surface area of the fin, m^2
A_j	lateral surface area of the jth sub-fin region, m^2
$[A]$	global conduction matrix
C	parameter
C_p	specific heat of moist air, J/(kg K)
$[K]$	global conduction matrix
$[F]$	force matrix
$h(X)$	overall heat-transfer coefficient, W/(m^2 K)
$h(X, Y)$	overall heat-transfer coefficient, W/(m^2 K)
$\bar{h}$	average overall heat-transfer coefficient, W/(m^2 K)
h_i	overall heat-transfer coefficient at $x = x_i$, W/(m^2 K)
$\bar{h}_j$	average overall heat-transfer coefficient on the jth sub-fin region, W/(m^2 K)
h_s	sensitive heat-transfer coefficient, W/(m^2 K)
i_{fg}	latent heat of water condensate, J/kg
K_m	mass transfer coefficient, kg/(s m^2)
k_f	thermal conductivity of the fin, W/(m K)
L	fin height or side length of a square plate fin, m
ℓ	distance between two neighboring nodes in the x- and y-directions
$m(x)$	dimensionless parameter, $\frac{2L^2h(X)}{k_f\delta}$
$m(x,y)$	dimensionless parameter, $\frac{2L^2h(X,Y)}{k_f\delta}$
$\bar{m}_j$	dimensionless parameter on the jth sub-fin region, $\frac{2L^2\bar{h}_j}{k_f\delta}$
N	number of the measured temperatures in the fin or sub-fin regions
N_x	number of nodes in the x-direction
N_y	number of nodes in the y-direction
P	number of sub-space intervals
Q	total heat-transfer rate dissipated from the fin, W
q_j	heat-transfer rate dissipated from the jth sub-fin region, W
RH	relative humidity
T	fin temperature, K
T_a	air ambient temperature, K
T_b	fin base temperature, K
T_m	measured fin temperature at $x = x_m$, K
T_j	measured fin temperature in the jth sub-fin region, K
$[T]$	global temperature matrix
V_{air}	frontal air speed, m/s
X, Y	spatial coordinates, m
x, y	dimensionless spatial coordinates
x_m	measurement location

Greek symbols

δ	fin thickness, m
η_f	wet fin efficiency
ω_j	random error
ω_a	air humidity ratio
ω_f	humidity ratio evaluated at the fin temperature.
θ	dimensionless fin temperature, $(T - T_a)/(T_b - T_a)$
$[\theta]$	global temperature matrix

Superscripts

cal	calculated value
exa	exact value
mea	measured data

the temperature of the whole fin is lower than the dew point temperature of the surrounding air. The partially wet surface occurs when the dew point temperature is lower than the fin tip temperature and is higher than the fin base temperature. If the temperature of the whole fin is higher than the dew point temperature, the fin is fully dry. As stated by Liang et al. [3], the condensation of the moist air along the fin surface reduced the fin efficiency. In order to determine the wet fin efficiency, it is necessary to model the combined heat and mass transfers on the cooling surface in detail. It is known that the heat transfer on the fin is closely related to the airflow pattern. Velayati and Yaghoubi [4] applied a numerical method to investigate convective heat transfer from an array of parallel bluff plates. It can be found from Ref. [4] that there exhibited very complex three-dimensional flow characteristics within parallel bluff plates. This complex flow pattern is accompanied by fluid separation and reattachment. This can cause local variation of the heat-transfer coefficient on the dry fin. It was demonstrated by Saboya and Sparrow [5] that the sensitive heat-transfer coefficient can vary by a factor of 50 over a plate fin in a one-tube-row plate finned-tube heat exchanger. It was found that the measured fin efficiency was less than the calculated result assuming a uniform heat transfer coefficient [3]. Moreover, the calculated results of Saboya and Sparrow [5], Chen et al. [6], Chen and Chou [7,8] and Chen and Hsu [9] also showed that the heat-transfer coefficient on the fin inside the plate finned-tube heat exchangers was non-uniform under dry conditions. On the other hand, the conventional analysis assuming the uniform heat-transfer coefficient on the fin seems to be inadequate. This implies that the actual steady-state heat-transfer coefficient on a fin for the present problem should be the function of position. However, due to the difficulty of considering variable sensible heat-transfer coefficient, a uniform sensible heat-transfer coefficient was often assumed by many investigators in order to determine the wet fin efficiency [3].

Lin and Jang [2] applied the second-order central-difference scheme to investigate a two-dimensional fin efficiency

analysis of combined heat and mass transfers in elliptic fins. Liang et al. [3] made a comparison of one-dimensional (1-D) and two-dimensional (2-D) models for the wet fin efficiency of a plate-fin-tube heat exchanger using the fourth-order Runge–Kutta method and a second-order central-difference scheme. It is worth noting that the fin efficiency of a 2-D rectangular plate-fin was approximated by a 1-D equivalent annular circular fin having the same surface area. Their results [3] showed that the wet fin efficiency obtained from the 1-D model agreed with that obtained from the 2-D model. Chen [10] applied a 2-D model to analyze the fin performance with heat transfer and mass transfer in cooling and dehumidifying processes. In this work, the effect of the moist air temperature and relativity humidity (RH) on the fin performance was considered. His results showed that the wet fin efficiency was sensitive to the RH value. Lin et al. [11] applied a 1-D model in conjunction with an experimental study to investigate the performance of a square fin under wet conditions. Their experimental results showed that there existed the fully dry, very fine droplet, larger droplet and film-like regions on the fin. The distribution of the droplet on the fin can be random and non-uniform. The measured fin temperatures in the upstream sub-fin regions were lower than those in the downstream sub-fin regions under the condition of the same fin height. However, in order to simplify the problem considered, the sensible heat-transfer coefficient was assumed to be constant over the fin, and the Lewis number was also assumed to be unity. It was a pity that a comparison between their calculated and experimental fin temperatures was not made. It can be found from Ref. [12] that the measurements of the local heat-transfer coefficient on a plate fin under steady-state heat-transfer conditions were very difficult to perform, since the local fin temperature and local heat flux were required. Thus the wet fin efficiency was often determined under the assumptions of the uniform sensible heat-transfer coefficient and the given functional relation between the relative humidity and fin temperature [1–3,10,11,13,14]. Liang et al. [3] and Lin et al. [11] applied the model of McQuiston [15] to determine the wet fin efficiency. Virtually, various relations between "the difference of the humidity ratio evaluated at the fin temperature and air humidity ratio" and "the difference of the fin temperature and air ambient temperature", such as the quadratic functional form, can also be proposed [2,3,10,11,13,14]. In the present study, the sensible and overall heat-transfer coefficients, the Lewis number and the functional relation between the relative humidity and fin temperature are assumed to be unknown. The main purposes of the present study is to estimate the average overall heat-transfer coefficient and wet fin efficiency under wet conditions using experiment temperature data given by Lin et al. [11]. In order to validate the reliability and accuracy of the present inverse scheme, a comparison of the overall heat-transfer between the present estimates obtained from the 1-D and 2-D models and exact values is made using simulated temperature data. Rosario and Rahman [16] analyzed the heat transfer in partially wet annular fin assembly during the process of dehumidification.

As stated by Lin et al. [11], the effect of the RH value on the fully wet fin efficiency of extended surface was very confusing. Threlkeld's model [17] showed that the wet fin efficiency was slightly affected by the RH value. ARI 410-91 standard [18] was based on the 1-D analysis given by Ware and Hacha [19]. It can be found from Ref. [11] that the fully wet fin efficiency obtained from this standard [18] was independent of the relative humidity under fully wet conditions. Conversely, the works of Chen [10], Elmahdy and Biggs [13], McQuiston [15] and Rosario and Rahman [16] showed that the fully wet fin efficiency significantly decreased with increasing the RH value. Thus another purpose of the present study is to investigate the relation of the wet fin efficiency and the relative humidity. It is known that the accuracy of the estimated overall heat-transfer coefficient has a great effect on the wet fin efficiency. Thus the estimation of a more accurate overall heat-transfer coefficient on the fin is also an important task for the present problems.

Quantitative studies of the heat-transfer processes occurring in the industrial applications require accurate knowledge of the surface conditions and the thermal physical quantities of the material. It is well known that these physical quantities and the surface conditions can be predicted using the measured temperatures inside the test material. Such problems are called the inverse heat conduction problems that have become an interesting subject recently. To date, various inverse methods in conjunction with the measured temperatures inside the test material have been developed for the analysis of the inverse heat conduction problems [20,21]. However, to the authors' knowledge, a few investigators performed the prediction of the overall heat-transfer coefficient on the fin under wet conditions and wet fin efficiency using the inverse scheme because both heat transfer and mass transfer occurred simultaneously during the process of dehumidification.

Chen et al. [6], Chen and Chou [7,8] and Chen and Hsu [9], respectively applied the finite difference method in conjunction with the least-squares scheme and experimental temperature data to predict the average sensitive heat-transfer coefficient on the fin and fin efficiency inside one-tube plate finned-tube heat exchangers for various fin spacings in forced convection and free convection under dry conditions. The estimated results of the average sensitive heat-transfer coefficient on the fin in free convection agreed with those obtained from the correlations recommended by current textbooks [22,23]. This implies that the present inverse scheme has good accuracy and good reliability. Thus the similar inverse scheme [6–9] is applied to investigate the present 2-D problem.

The whole fin is first divided into several analysis sub-fin regions in the present study before performing the inverse calculation. Later, the finite difference method in conjunction with experimental measured temperatures given by Lin et al. [11] and least-squares method is applied to predict the

average overall heat-transfer coefficients on these sub-fin regions. Furthermore, the average overall heat-transfer coefficient on a fin under wet conditions and wet fin efficiency can be obtained for various air speeds and RH values. The effects of the relative humidity and air speed on the estimation of the overall heat-transfer coefficient and wet fin efficiency under wet conditions will also be investigated. The computational procedure for the estimates of the overall heat-transfer coefficients on each sub-fin region is performed repeatedly until the sum of the squares of the deviations between the calculated and measured temperatures becomes minimum.

2. Mathematical formulation

A one-dimensional (1-D) inverse heat conduction problem is first introduced to estimate the unknown overall heat-transfer coefficient under wet conditions and wet fin efficiency. The physical geometry of the one-dimensional inverse problem is shown in Fig. 1. The mathematical formulation, basic assumptions and experimental temperature data used in this study come from the work of Lin et al. [11]. For the direct heat conduction problems, the temperature field can be determined provided that the overall heat-transfer coefficient $h(X)$ is given. However, the overall heat-transfer coefficient is not known for the inverse heat conduction problems (IHCP). It cannot be estimated unless additional information of the measured fin temperatures at various measurement locations in the test material is given. In this study, the thermocouples are fixed at several different locations in order to record their temperatures. The IHCP investigated here involve the estimates of the unknown overall heat-transfer coefficient and wet fin efficiency from the measured fin temperatures at various measurement locations. The governing differential equation is expressed as [11]

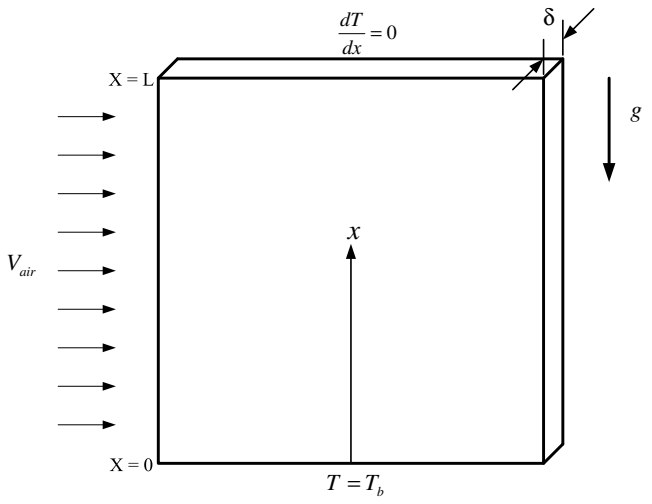

Fig. 1. Physical geometry of the 1-D inverse problem.

$$k_f\delta\frac{d^2T}{dX^2} - 2[h_s(X)(T-T_a) + i_{fg}K_m(\omega_f-\omega_a)] = 0 \quad \text{for } 0<X<L \tag{1}$$

where T is the fin temperature. T_a is the air ambient temperature. X denotes the spatial coordinate. L is the fin height. δ is the fin thickness. K_f is the thermal conductivity of the fin. h_s is the sensible heat-transfer coefficient. i_{fg} denotes the latent heat of water condensate. K_m denotes the mass transfer coefficient. ω_a is the air humidity ratio. ω_f is the humidity ratio evaluated at the fin temperature.

Various relations between "$\omega_f-\omega_a$" and "$T-T_a$" can be proposed [3,10,11,13,14]. On the other hand, their relationship cannot be linear. Coney et al. [14] assumed that the functional relation between "$\omega_f-\omega_a$" and "$T-T_a$" was a second-order polynomial function. However, in order to compare with the results given by Lin et al. [11], the relation between "$\omega_f-\omega_a$" and "$T-T_a$" in the present study can be assumed as

$$\omega_f-\omega_a = C(T-T_a) \tag{2}$$

where the parameter C is not always a constant in the present study C_p is the specific heat of moist air.

Substituting Eq. (2) into Eq. (1) yields

$$\frac{d^2T}{dX^2} - \frac{2h(X)}{k_f\delta}(T-T_a) = 0 \quad \text{for } 0<X<L \tag{3}$$

where $h(X)$ is the overall heat-transfer coefficient for the 1-D model and can be expressed as

$$h(X) = h_s(X) + i_{fg}K_mC \tag{4}$$

Obviously, this overall heat-transfer coefficient involves the sensible heat-transfer coefficient and that due to mass transfer. As stated by Liang et al. [3], it is difficult to determine the parameter C. Coney et al. [14] indicated that the overall heat-transfer coefficient was related to the fin temperature, $h(X)$ and the h_s value might not be regarded as the constant values simultaneously. This implies that the parameter C can be the function of X for the 1-D model.

As stated by Lin et al. [11], most of the investigators applied the Chilton–Colburn analogy to perform their studies. The Chilton–Colburn analogy [24] was expressed as

$$\frac{h_s}{K_mC_p} = Le^{2/3}$$

where Le is the Lewis number. It is worth noting that Le is not assumed to be unity in the present study. C_p is the specific heat of moist air.

The corresponding boundary conditions of this problem are

$$T(0) = T_b \tag{5}$$

and

$$\frac{dT}{dX} = 0 \quad \text{at } X = L \tag{6}$$

where T_b is the fin base temperature.

The "insulated tip" assumption can be an adequate approximation provided that the actual heat-transfer rate dissipated through the fin tip is much smaller than the total heat-transfer rate drawn from the base wall [7–9,25]. For simplicity, the average overall heat-transfer coefficient on the tip surface of the fin can be assumed to be the same as that on the lateral surfaces of the fin. This implies that the "insulated tip" assumption in the present study can be reasonable provided the ratio of the surface area of the fin tip to the total fin surface area, $\frac{\delta}{2L+\delta}$, is very small. Based on experiment data of the present study, the surface area of the fin tip is only 0.9% of the total fin surface area for $L = 10$ cm and $\delta = 0.2$ cm. Thus the assumption of Eq. (6) should be reasonable.

For convenience of the inverse analysis, the following dimensionless parameters are introduced as

$$x = \frac{X}{L},\ m(x) = \frac{2L^2 h(X)}{k_f \delta} \quad \text{and} \quad \theta = \frac{T - T_a}{T_b - T_a} \tag{7}$$

Introducing these dimensionless variables in Eq. (7) into Eqs. (3), (5) and (6) leads to the following dimensionless equations:

$$\frac{d^2\theta}{dx^2} - m(x)\theta = 0, \quad 0 < x < 1 \tag{8}$$

$$\theta(x) = 1, \quad \text{at } x = 0 \tag{9}$$

and

$$\frac{d\theta}{dx} = 0, \quad \text{at } x = 1 \tag{10}$$

However, it can be found from Fig. 4 of Ref. [11] that the measured fin temperatures on the downstream sub-fin regions were markedly higher than those on the upstream sub-fin regions for various air speeds under the conditions of the same fin height, relative humidity, fin base temperature T_b and ambient temperature T_a. This implies that the application of the 1-D model to the present problem may not be very reasonable. Moreover, there exhibited the recirculating flows of the airflow coming into the region between two parallel fins [4] and the random distribution of the droplets on the fin under wet conditions [11]. Thus a 2-D inverse heat conduction problem is introduced to estimate the unknown overall heat-transfer coefficient and wet fin efficiency under wet conditions. Fig. 2 shows the physical geometry of the two-dimensional inverse problem with measurement locations and sub-fin regions, where L denotes the side length of the square plate fin. Due to the thin fin behavior, the temperature gradient in the Z-direction (the fin thickness) is small and the fin temperature varies only in the X- and Y-directions. It is known that the heat-transfer coefficient on the fin inside the plate fin heat exchangers under dry conditions was non-uniform [5–9]. Thus the overall heat-transfer coefficient $h(X, Y)$ for the 2-D model is also assumed to be non-uniform. Similarly, this overall heat-transfer coefficient $h(X, Y)$ can be estimated provided that the fin temperatures at several different measurement locations can be measured. The present study applies the similar inverse scheme [6–9] in conjunction with experimental measured temperatures given by Lin et al. [11] to estimate the unknown average overall heat-transfer coefficient and wet fin efficiency under wet conditions in forced convection. Under the assumptions of the steady-state and constant thermal properties, the 2-D heat conduction equation for the thin plate fin can be expressed as

$$\frac{\partial^2 T}{\partial X^2} + \frac{\partial^2 T}{\partial Y^2} = \frac{h_s(X, Y)}{k_f t}(T - T_a) + \frac{i_{fg} K_m(\omega_f - \omega_a)}{k_f t} \tag{11}$$

Its corresponding boundary conditions are

$$\frac{\partial T}{\partial Y} = 0 \quad \text{at } Y = 0 \text{ and } Y = L \tag{12}$$

$$T(0, Y) = T_o \tag{13}$$

$$\frac{\partial T}{\partial X} = 0 \quad \text{at } X = L \tag{14}$$

where X and Y are the spatial coordinates. T, k_f, h_s, i_{fg}, K_m, ω_a and ω_f have been defined in Eq. (1). Based on experiment data of the present study and the assumption of the insulated tip, the ratio of the surface area of the fin tip to the total fin surface area, $\frac{3L\delta}{2L^2+3L\delta}$, is only 2.91% for $L = 10$ cm and $\delta = 0.2$ cm. This also implies that the assumption of Eqs. (12) and (14) is reasonable.

However, in order to compare with the results obtained from the 1-D model, the relation between "$\omega_f - \omega_a$" and "$T - T_a$" shown in Eq. (2) is also used. Thus substituting Eq. (2) into Eq. (11) yields the following form as

$$\frac{\partial^2 T}{\partial X^2} + \frac{\partial^2 T}{\partial Y^2} = \frac{2h(X, Y)}{k_f \delta}(T - T_a) \quad \text{for } 0 < X < L, 0 < Y < L \tag{15}$$

where $h(X, Y)$ is the unknown overall heat-transfer coefficient for the 2-D model and can be expressed as

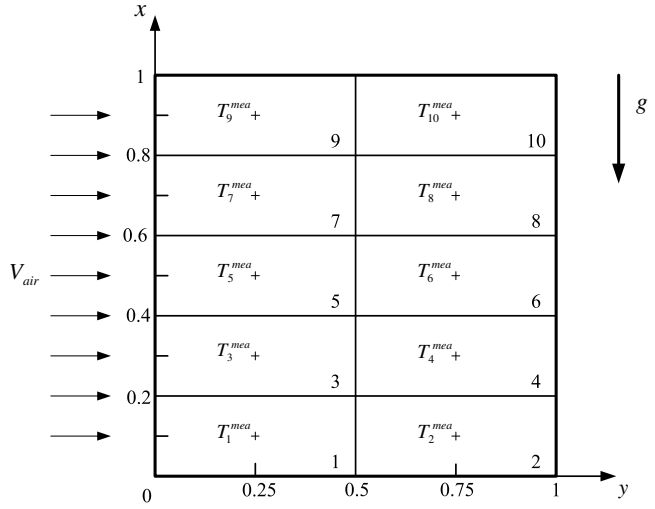

Fig. 2. Physical geometry of the 2-D inverse problem with measurement locations and sub-fin regions.

$$h(X,Y) = h_s(X,Y) + i_{fg}K_m C \tag{16}$$

Similarly, the functional relation between "$\omega_f - \omega_a$" and "$T - T_a$" is not known in the present study. On the other hand, the parameter C in Eq. (16) can be the function of X and Y for the 2-D model. It is obvious that the functional form of the parameter C for the 2-D model is different from that for the 1-D model, as shown in Eq. (4).

For convenience of the inverse analysis, the following dimensionless parameters are introduced as:

$$x = X/L, \quad y = Y/L, \quad \theta = \frac{T - T_a}{T_b - T_a} \quad \text{and}$$

$$m(x,y) = m_r = \frac{2L^2 h(X,Y)}{k_f \delta} \tag{17}$$

Substitution of Eq. (17) into Eqs. (11)–(14) gives the following equations:

$$\frac{\partial^2\theta}{\partial x^2} + \frac{\partial^2\theta}{\partial y^2} = m(x,y)\theta \tag{18}$$

$$\frac{\partial\theta}{\partial y} = 0 \quad \text{at } y = 0 \text{ and } y = 1 \tag{19}$$

$$\theta = 1 \quad \text{at } x = 0 \tag{20}$$

and

$$\frac{\partial\theta}{\partial x} = 0 \quad \text{at } x = 1 \tag{21}$$

3. Numerical analysis

3.1. One-dimensional model

The application of the central-difference method to Eq. (8) can produce the following difference equation as:

$$\frac{\theta_{i-1} - 2\theta_i + \theta_{i+1}}{\ell^2} - m(x_i)\theta_i = 0 \quad \text{for } i = 2,3,\ldots,N_x \tag{22}$$

where n is the nodal number. $\ell = 1/(N_x - 1)$ denotes the distance between two neighboring nodes in the x-direction and is uniform. $m(x_i)$ denotes the dimensionless value at $x = x_i$.

The discretized form at $x = 0$ is expressed as

$$\theta_1 = 1 \tag{23}$$

The application of the central-difference approximation to the boundary condition (10) can yield the difference equation as

$$\theta_{n-1} = \theta_{n+1} \tag{24}$$

Substitution of Eq. (24) into Eq. (22) yields the difference equation as

$$\frac{2}{\ell^2}\theta_{n-1} - \left[\frac{2}{\ell^2} + m(1)\right]\theta_n = 0 \tag{25}$$

Rearrangement of Eqs. (22), (23) and (25) can yield the matrix equation as

$$[K][\theta] = [F] \tag{26}$$

where $[K]$ is the $(N_x - 1) \times (N_x - 1)$ global conduction matrix. $[\theta]$ is the $(N_x - 1) \times 1$ matrix representing the nodal temperatures. $[F]$ is the $(N_x - 1) \times 1$ force matrix. The nodal temperatures can be obtained from Eq. (26) using the Gauss elimination algorithm.

Once the unknown overall heat-transfer coefficient $h(X)$ is obtained, the average overall heat-transfer coefficient $\bar{h}$ and total heat-transfer rate dissipated from the whole fin to the ambient Q can be determined using the following expressions.

The exact value of the average overall heat-transfer coefficient $\bar{h}$ under wet conditions for the 1-D and 2-D models can respectively be expressed as

$$\bar{h} = \frac{\int_0^L h(X)\,dX}{L} \quad \text{and} \quad \bar{h} = \frac{\int_0^L \int_0^L h(X,Y)\,dX\,dY}{L^2} \tag{27}$$

The total heat-transfer rate dissipated from the whole fin to the ambient Q for the 1-D model can be written as

$$Q = 2\int_0^L h(X)(T_a - T)\,dX \tag{28}$$

The wet fin efficiency η_f is defined as the ratio of the actual heat-transfer rate from the fin to the dissipated heat rate from an ideal fin which the temperature of the whole fin is the same as the fin base temperature T_b. Thus the fin efficiency η_f for the 1-D model can be expressed as

$$\eta_f = \frac{Q}{2\bar{h}L(T_a - T_b)} \tag{29}$$

In order to estimate the unknown overall heat-transfer coefficient $h(X)$, additional information of the steady-state measured temperatures at N interior measurement locations is required. The more a number of the analysis subspace intervals are, the more accurate the estimation of the unknown overall heat-transfer coefficient can be. Relatively, a more computational time can be required.

The functional form of the unknown overall heat-transfer coefficient $h(X)$ in the present study is assumed to be the function of X before performing the inverse calculation. However, it may not be easy to obtain an approximate polynomial function that can completely fit $h(X)$ for the whole space domain considered. Under this circumstance, the distribution of $h(X)$ can be approximated by a series of p connected cubic polynomial functions. The unknown overall heat-transfer coefficient on the kth analysis subintervals $h_k(X)$ can be expressed as

$$h_k(X) = \sum_{j=1}^{4} C_j X^{j-1}, \quad k = 1,\ldots,p \tag{30}$$

where C_j, $j = 1,2,\ldots,4$, are the unknown coefficients and can be estimated using the least-squares method in conjunction with the measured fin temperatures in each analysis sub-space interval.

Due to the application of the cubic spline, the mandatory constraints at the interface between two adjacent anal-

ysis sub-intervals must be satisfied and are expressed as [26,27]:

$$h_k = h_{k+1}, \quad h'_k = h'_{k+1} \quad \text{and} \quad h''_k = h''_{k+1}, \quad k = 1, 2, \ldots, p-1 \tag{31}$$

In practical applications, measured temperature profiles often exhibit random oscillations due to measurement errors [11,27–29]. On the other hand, due to experimental uncertainties, more realistic measured temperatures should add simulated small random errors to the exact data obtained from the solution of the related direct problem. Thus in order to simulate the measured temperature T_j^{mea} taken from the jth thermocouple, the exact value T_j^{mea} can be modified by adding a small random error. The measured temperature T_j^{mea} used in the present inverse analysis can be expressed as

$$T_j^{\text{mea}} = T_j^{\text{exa}}(1 + \omega_j) \quad \text{for } j = 1, 2, \ldots, N \tag{32}$$

where N denotes the number of the measured temperatures in the fin. ω_j is the random error generated by the QuickBAISC 4.50 and is assumed to be within -3% to 3% in the present study. The standard deviation of the mean of the measured temperatures with respect to the exact values is respectively defined as [26,27]:

$$\sigma^{\text{exa}} = \frac{1}{N}\left[\sum_{j=1}^{N}\left(T_j^{\text{mea}} - T_j^{\text{exa}}\right)^2\right]^{1/2}, \quad j = 1, 2, \ldots, N \tag{33}$$

It is easy to obtain the fin temperatures at several different measurement locations using the thermocouples. A curve-fitted profile generated through a least-squares process can be used to fit experimental fin temperature data before performing the inverse calculations. Later, the measured fin temperatures T_j^{mea}, $j = 1, 2, \ldots, N$, can be obtained from this curve-fitted profile. Thus the unknown overall heat-transfer coefficient $h(X)$ can be obtained using these measured fin temperatures.

The least-squares minimization technique is applied to minimize the sum of the squares of the deviations between the calculated and measured fin temperatures at selected measurement locations. The error in the estimates $E(C_1, C_2, \ldots, C_{M_t})$ for the 1-D model can be expressed as

$$E(C_1, C_2, \ldots, C_{M_t}) = \sum_{j=1}^{M_t}\left[T_j^{\text{cal}} - T_j^{\text{mea}}\right]^2 \tag{34}$$

where M_t denotes the number of the unknown coefficients. It is obvious that the M_t value is equal to "$p + 3$" in the present study. T_j^{cal} denotes the calculated temperature at $x = x_j$. The estimated values of C_j, $j = 1, 2, \ldots, M_t$, can be determined provided that the values of $E(C_1, C_2, \ldots, C_{M_t})$ are minimum. The detailed computational procedures for estimating the unknown coefficients C_j can be found in Refs. [26,27]. In order to avoid repetition, they are not shown in this manuscript. The computational procedures of the present study are repeated until the values of $\left|\frac{T_j^{\text{mea}} - T_j^{\text{cal}}}{T_j^{\text{mea}}}\right|$ for $j = 1, 2, \ldots, M_t$ are all less than 10^{-5}.

3.2. Two-dimensional model

In the present study, the whole fin is divided into N sub-fin regions. Later, the overall heat-transfer coefficient on each sub-fin region is assumed to be constant. The application of the finite difference method to Eq. (18) can produce the following difference equation on the kth sub-fin region as:

$$\frac{\theta_{i+1,j} - 2\theta_{i,j} + \theta_{i-1,j}}{\ell^2} + \frac{\theta_{i,j+1} - 2\theta_{i,j} + \theta_{i,j-1}}{\ell^2} = \bar{m}_k\theta_{i,j} \quad \text{for } i = 1, 2, \ldots, N_x, j = 1, 2, \ldots, N_y \quad \text{and} \quad k = 1, 2, \ldots, N \tag{35}$$

where N_x and N_y are the nodal numbers in x- and y-directions, respectively. ℓ is the distance between two neighboring nodes in the x- and y-directions and is defined as $\ell = 1/(N_x - 1) = 1/(N_y - 1)$. $\bar{m}_k$ denotes the unknown dimensionless parameter on the kth sub-fin region and is defined as $\bar{m}_k = 2L^2\bar{h}_k/(k\delta)$, where $\bar{h}_k$ denotes the average overall heat-transfer coefficient on the kth sub-fin region.

The finite difference forms of the boundary conditions (19)–(21) can be written as

$$\theta_{i,2} = \theta_{i,0} \quad \text{and} \quad \theta_{i,N_y-1} = \theta_{i,N_y+1} \quad \text{for } i = 1, 2, \ldots, N_x \tag{36}$$

$$\theta_{i,j} = 1 \quad \text{and} \quad \theta_{N_x-1,j} = \theta_{N_x+1,j} \quad \text{for } j = 1, 2, \ldots, N_y \tag{37}$$

Substitution of Eqs. (36) and (37) into Eq. (35) can obtain the difference equations at the boundary surfaces as

$$\frac{\theta_{i+1,1} - 2\theta_{i,1} + \theta_{i-1,1}}{\ell^2} + \frac{2\theta_{i,2} - 2\theta_{i,1}}{\ell^2} = \bar{m}_k\theta_{i,1} \quad \text{for } k = 1, 3, 5, 7, 9 \tag{38}$$

$$\frac{\theta_{i+1,N_y} - 2\theta_{i,N_y} + \theta_{i-1,N_y}}{\ell^2} + \frac{-2\theta_{i,N_y} + 2\theta_{i,N_y-1}}{\ell^2} = \bar{m}_k\theta_{i,N_y} \quad \text{for } k = 2, 4, 6, 8, 10 \tag{39}$$

$$\frac{-2\theta_{N_x,j} + 2\theta_{N_x-1,j}}{\ell^2} + \frac{\theta_{N_x,j+1} - 2\theta_{N_x,j} + \theta_{N_x,j-1}}{\ell^2} = \bar{m}_k\theta_{N_x,j} \quad \text{for } k = 9, 10 \tag{40}$$

The difference equations for the nodes at the interface between two neighboring sub-fin regions, as shown in Fig. 3, are given as

$$\frac{\theta_{i+1,j} - 2\theta_{i,j} + \theta_{i-1,j}}{\ell^2} + \frac{\theta_{i,j+1} - 2\theta_{i,j} + \theta_{i,j-1}}{\ell^2} - \frac{\bar{m}_k + \bar{m}_{k+1}}{2}\theta_{i,j} = 0 \quad \text{for } k = 1, 3, \ldots, 9 \tag{41}$$

and

$$\frac{\theta_{i+1,j} - 2\theta_{i,j} + \theta_{i-1,j}}{\ell^2} + \frac{\theta_{i,j+1} - 2\theta_{i,j} + \theta_{i,j-1}}{\ell^2} - \frac{\bar{m}_k + \bar{m}_{k+2}}{2}\theta_{i,j} = 0 \quad \text{for } k = 1, 2, \ldots, 8 \tag{42}$$

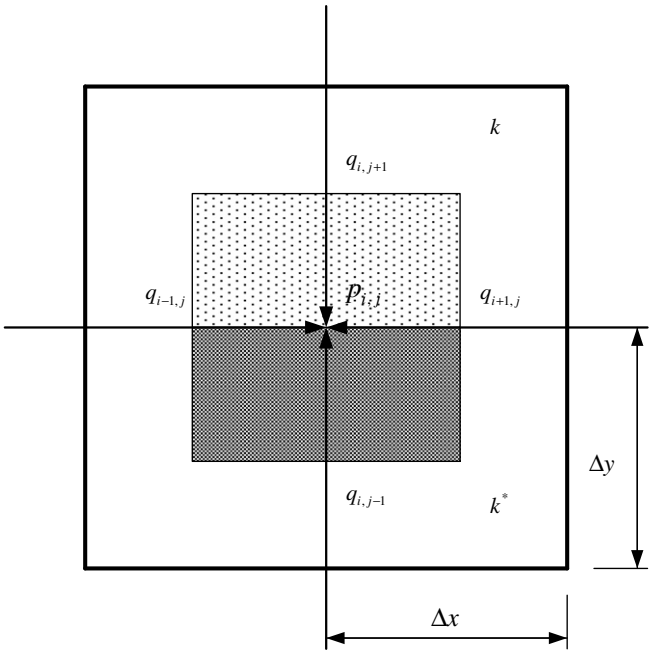

Fig. 3. Nodes for the interface of two neighboring sub-fin regions.

The difference equations for the nodes between four neighboring sub-fin regions are given as

$$\frac{\theta_{i+1,j}-2\theta_{i,j}+\theta_{i-1,j}}{\ell^2}+\frac{\theta_{i,j+1}-2\theta_{i,j}+\theta_{i,j-1}}{\ell^2} - \frac{\bar{m}_k+\bar{m}_{k+1}+\bar{m}_{k+2}+\bar{m}_{k+3}}{4}\theta_{i,j} = 0 \quad \text{for } k=1,3,5,7 \tag{43}$$

Rearrangement of Eqs. (35) and (38)–(43) can yield the similar matrix equation shown in Eq. (26). However, the elements in $[K]$, $[\theta]$ and $[F]$ for the 2-D model are different from those for the 1-*D* model.

Under the assumption that the unknown overall heat-transfer coefficient on each sub-fin region is approximated by a constant value, the heat transfer rate dissipated from the *j*th sub-fin region q_i can be expressed as

$$q_i = 2\bar{h}_j \int_{A_j} (T - T_a)\,\mathrm{d}A \quad \text{for } j=1,2,\ldots,N \tag{44}$$

The average overall heat-transfer coefficient on the fin $\bar{h}$ under wet conditions for the 2-D model can be expressed as

$$\bar{h} = \sum_{j=1}^{N} \bar{h}_j A_j \Big/ A_f \tag{45}$$

where N is the number of the sub-fin regions. A_f is the lateral surface area of the fin.

As stated by Rosario and Rahman [16], the actual total heat-transfer must include both the sensible heat transfer and latent heat transfer originated by the mass transfer during the process of dehumidification. The sensible heat transfer is due to convection from the air to the fin because of the temperature difference between the air and the fin. The latent heat transfer is caused by the humidity ratio difference between the air and the fin surface. Thus the wet fin efficiency η_f for the 2-D model can be expressed as [3,6–9,16]

$$\eta_f = \frac{\sum_{j=1}^{N} q_j}{2A_f(T_a - T_b)\bar{h}} \tag{46}$$

The actual total heat-transfer rate dissipated from the fin to the ambient Q for the 2-D model can be written as

$$Q = \sum_{j=1}^{N} q_j \tag{47}$$

In order to estimate the unknown overall heat-transfer coefficient $\bar{h}_j$ on the *j*th sub-fin region, additional information of steady-state measured fin temperatures is required at N interior measurement locations. The measured fin temperature taken from the *j*th thermocouple is denoted by T_j^{mea}. The error in the estimates $E(\bar{m}_1,\bar{m}_2,\ldots,\bar{m}_N)$ for the 2-D model is minimized and is defined as

$$E(\bar{m}_1,\bar{m}_2,\ldots,\bar{m}_N) = \sum_{j=1}^{N}\left[T_j^{cal} - T_j^{mea}\right]^2 \tag{48}$$

where the unknown average overall heat-transfer coefficients on each sub-fin region $\bar{h}_j$, $j=1,2,\ldots,N$, can be obtained from the definition of $\bar{m}_j$. The calculated fin temperature taken from the *j*th thermocouple location, T_j^{cal}, is taken from the similar matrix equation shown in Eq. (26).

The estimated values of $\bar{m}_j$, $j=1,2,\ldots,N$, are determined until the value of $E(\bar{m}_1,\bar{m}_2,\ldots,\bar{m}_N)$ is minimum. The detailed computational procedures for estimating the unknown value $\bar{m}_j$ can be found in Refs. [6–9]. In order to avoid repetition, they are not shown in this manuscript. The computational procedures for the 2-D model are also repeated until the values of $\left|\frac{T_j^{mea}-T_j^{cal}}{T_j^{mea}}\right|$ for $j=1,\ 2,\ldots,\ N$ are all less than 10^{-5}. Once the $\bar{m}_j$ values, $j=1,2,\ldots,N$, are determined, the average overall heat-transfer coefficient $\bar{h}$, total heat-transfer rate Q and wet fin efficiency η_f under wet conditions can be obtained from Eqs. (45)–(47).

4. Results and discussion

In order to demonstrate the accuracy and reliability of the present inverse scheme, two numerical examples and an experimental example using experimental data given by Lin et al. [11] are illustrated. Thus the least-squares fitting method is applied to fit experimental measured fin temperatures given by Lin et al. [11]. The data used in the present study come from the work of Lin et al. [11]. Thus the data taken for the inverse analysis are: $k=177$ W/m °C, $\delta=0.002$ m, $L=0.1$ m, $T_a=300.15$ K and $T_b=282.15$ K. The measured fin temperature $T(X)$ for the 1-D model is defined as the average of the fin temperatures at the measurement locations (X, $Y=0.25$ L) and

($X, Y = 0.75L$) shown in Fig. 4 of Ref. [11]. Comparisons among the present estimates, the exact values and an experimental result given by Lin et al. [11] are made.

4.1. Numerical example

In order to validate the accuracy and reliability of the present inverse method, two examples with the overall heat-transfer coefficient $h(X) = 50e^{X}$ for the 1-D inverse heat conduction problem and $h(X, Y) = 1000XY$ for the 2-D inverse problem are illustrated. The inverse problems considered here are concerned with the estimations of the unknown average overall heat-transfer coefficient $\bar{h}$ for $h(X) = 50e^{X}$ and $h(X, Y) = 1000XY$. In order to predict the $\bar{h}$ value, additional measured fin temperatures taken at various interior measurement locations require to be obtained from the related direct problems. The nodal number N_x used in the computation of the 1-D model is $N_x = 11$. Four measurement locations 0.02 m, 0.04 m, 0.06 m and 0.08 m are needed to record the measured temperatures for the inverse problem with $h(X) = 50\ e^{X}$ and $p = 1$. However, five measurement locations 0.02 m, 0.04 m, 0.06 m, 0.07 m and 0.08 m are taken for $p = 2$. The unknown function $h(X)$ on each analysis sub-interval can be expressed as Eq. (30). Thus the values of C_j for $j = 1, 2, \ldots, M_t$ will be predicted. The unknown coefficients C_j for $j = 1, 2, \ldots, M_t$ used to begin the iterations are taken as unity. In order to investigate the effect of the number of analysis sub-intervals p on the present estimates, Table 1 displays the comparison of $h(X)$ at various nodes and $\bar{h}$ between the present estimates and exact values for the 1-D model and various p and ω_j values. The results show that the present estimates of $h(X)$ at various nodes and $\bar{h}$ show no obvious deviations for $p = 1$ and 2 and agree well with the exact values. The relative error of the $\bar{h}$ value is about 0.06% for the 1-D model, $\omega_j = 0$ and $p = 1$. Thus $p = 1$ is taken for all the following inverse calculations of the 1-D model through this illustrative example. The present estimates of $h(X)$ at various nodes slightly deviate from the exact value for $\omega_j = 0.4\%$. The maximum relative error of h(X) between the present estimates and exact values is about 4.6%. However, the relative error of the $\bar{h}$ value between the present estimate and exact value is about 0.77%. This implies that the present inverse method not only can obtain good estimates but also can reduce the amount of the measurement locations needed for the inverse calculation of the 1-D model. The initial guesses can be insensitive to the present estimates. Thus the effect of the initial guesses is not investigated in the present study.

Ten measurement locations are needed to record the measured temperatures for the inverse problem with $h(X, Y) = 100\ XY$. The nodal numbers N_x and N_y used in the computation of the 2-D model are $N_x = N_y = 21$. The unknown $\bar{m}_j$ value on the jth sub-fin region for $j = 1, 2, \ldots, N$ will be predicted. The unknown coefficients $\bar{m}_j$ for $j = 1, 2, \ldots, N$ used to begin the iterations are taken as unity. Table 2 displays the comparison of the unknown average overall heat-transfer coefficient $\bar{h}_j$ on the jth sub-fin region and average overall heat-transfer coefficient $\bar{h}$ between the present estimates and exact values for measurement error $\omega_j = 0$. It is found that the present estimates of $\bar{h}_j$ and $\bar{h}$ agree well with the exact values for $\omega_j = 0$. Table 3 shows the comparison of the $\bar{h}_j$ and $\bar{h}$ values between the present estimates and exact values for $\omega_j = 0.4\%$ and the 2-D model. The results show that the present estimates of $\bar{h}_j$ and $\bar{h}$ slightly deviate from the exact value for $\omega_j = 0.4\%$, too. The maximum relative error of the $\bar{h}_j$ value between the present estimates and exact value is about 4.6%. However, the relative error of the $\bar{h}$ value the present estimate and exact value is about 0.24% for $\omega_j = 0.4\%$. This implies that the present inverse scheme can also obtain good estimates for the 2-D model.

4.2. Experimental example

The main purpose of this study is to apply experimental data given by Lin et al. [11] to estimate the unknown average overall heat-transfer coefficient $\bar{h}$, total heat-transfer

Table 1
Comparison of the heat-transfer coefficient for $h(X) = 50\exp(X)$ and various p and ω_j values

X (m)	$h(X)$ (W/m^2 K)				$\bar{h}$ (W/m^2 K)			
	Present estimate			Exact value	Present estimate			Exact value
	$p = 1$		$p = 2$		$p = 1$		$p = 2$	
	$\omega_i = 0$	$\omega_i = 0.4\%$	$\omega_i = 0$		$\omega_i = 0$	$\omega_i = 0.4\%$	$\omega_i = 0$	
0.01	50.395	48.443	50.480	50.503	52.554	52.184	52.570	52.588
0.02	51.968	49.131	51.002	51.010				
0.03	51.532	50.146	51.517	51.523				
0.04	52.085	51.349	52.035	52.041				
0.05	52.625	52.601	52.571	52.564				
0.06	53.150	53.761	53.129	53.092				
0.07	53.657	54.691	53.682	53.625				
0.08	54.144	55.252	54.201	54.164				
0.09	54.609	55.304	54.651	54.709				
1.00	55.050	54.707	55.001	54.609				

Table 2
Comparison of the heat transfer coefficient for $h(X, Y) = 1000XY$, $m_j = 1$ and $\omega_j = 0$

T_j^{mea} (K)	$\bar{h}_j$(W/m^2 K)		$\bar{h}$(W/m^2 K)	
	Present estimate	Exact value	Present estimate	Exact value
$T_1^{mea} = 282.360$	$h_1 = 0.252$	$h_1 = 0.250$	2.500	2.500
$T_2^{mea} = 282.400$	$h_2 = 0.750$	$h_2 = 0.750$		
$T_3^{mea} = 282.763$	$h_3 = 0.750$	$h_3 = 0.750$		
$T_4^{mea} = 282.880$	$h_4 = 2.250$	$h_4 = 2.250$		
$T_5^{mea} = 283.111$	$h_5 = 1.249$	$h_5 = 1.250$		
$T_6^{mea} = 283.297$	$h_6 = 3.751$	$h_6 = 3.750$		
$T_7^{mea} = 283.371$	$h_7 = 1.750$	$h_7 = 1.750$		
$T_8^{mea} = 283.641$	$h_8 = 5.248$	$h_8 = 5.250$		
$T_9^{mea} = 283.512$	$h_9 = 2.250$	$h_9 = 2.250$		
$T_{10}^{mea} = 283.790$	$h_{10} = 6.751$	$h_{10} = 6.750$		

Table 3
Comparison of the heat transfer coefficient for $h(X, Y) = 1000XY$, $m_j = 1$ and $\omega_j = 0.4\%$

T_j^{mea} (K)	$\bar{h}_j$(W/m^2 K)		$\bar{h}$(W/m^2 K)	
	Present estimate	Exact value	Present estimate	Exact value
$T_1^{mea} = 282.342$	$h_1 = 0.246$	$h_1 = 0.250$	2.494	2.500
$T_2^{mea} = 282.401$	$h_2 = 0.763$	$h_2 = 0.750$		
$T_3^{mea} = 282.799$	$h_3 = 0.741$	$h_3 = 0.750$		
$T_4^{mea} = 282.847$	$h_4 = 2.238$	$h_4 = 2.250$		
$T_5^{mea} = 283.164$	$h_5 = 1.264$	$h_5 = 1.250$		
$T_6^{mea} = 283.201$	$h_6 = 3.753$	$h_6 = 3.750$		
$T_7^{mea} = 283.436$	$h_7 = 1.670$	$h_7 = 1.750$		
$T_8^{mea} = 283.463$	$h_8 = 5.259$	$h_8 = 5.250$		
$T_9^{mea} = 283.616$	$h_9 = 2.263$	$h_9 = 2.250$		
$T_{10}^{mea} = 283.631$	$h_{10} = 6.746$	$h_{10} = 6.750$		

rate Q and wet fin efficiency η_f under the assumption of constant thermal properties and wet conditions. Experiments proposed by Lin et al. [11] were performed in an environmental chamber, as shown in Fig. 1 of their work. The test apparatus was based on the air-enthalpy method proposed by ANSI/ASHARE Standard 33 [30]. The airflow measuring apparatus was constructed from ASHRAE Standard 41.2 [31]. Dry and wet bulb temperature measurement devices of the airflow were constructed based on ASHRAE Standard 41.1 [32]. Control resolution for the related dry and wet bulb temperatures was 0.1 °C. The material of the test fin was aluminum alloy 601. The test fin was 100 mm in length, 100 mm in width and 2 mm in thickness. The fin spacing was 3 mm. The thermocouple of type T was mounted at various measurement locations. The detailed locations of the thermocouples and the measured fin temperatures at various measurement locations were respectively shown in Figs. 2 and 4 of Ref. [11]. It can be observed from Fig. 4 of Ref. [11] that the experimental measured fin temperatures exhibited random oscillations. Thus the curve-fitted scheme is applied to fit these experimental fin temperature data over the whole space domain. Later, these curve-fitted temperatures are applied to perform the inverse analysis. Lin et al. [11] applied the

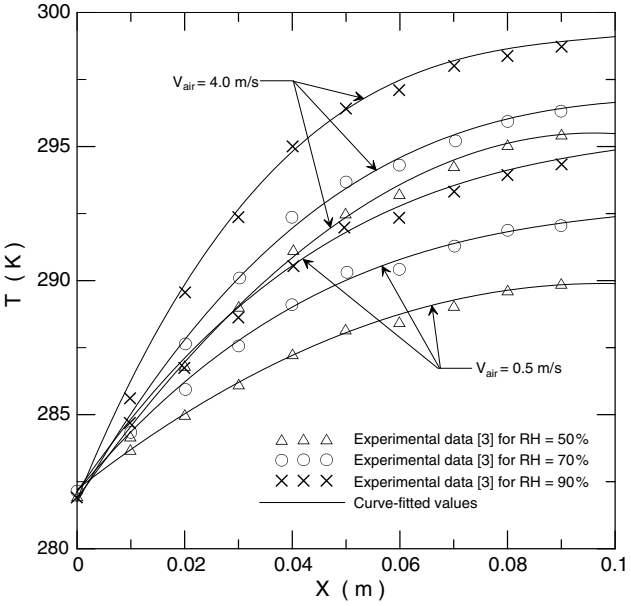

Fig. 4. Distributions of the curve-fitted fin temperatures and experimental fin temperatures given by Lin et al. [11] for various V_{air} and RH values.

1-D model to obtain the wet fin efficiency. However, the overall heat-transfer coefficient was not predicted.

Fig. 4 shows the distributions of the curve-fitted fin temperature and experimental fin temperature given by Lin et al. [11] for various V_{air} and RH values. The present inverse scheme in conjunction with these curve-fitted temperatures is applied to estimate the unknown overall heat-transfer coefficient $h(X)$ and wet fin efficiency η_f. Fig. 5 displays the comparison of the unknown overall heat-transfer coefficient $h(X)$ for RH = 50%, $V_{air} = 0.5$ m/s and various p values.

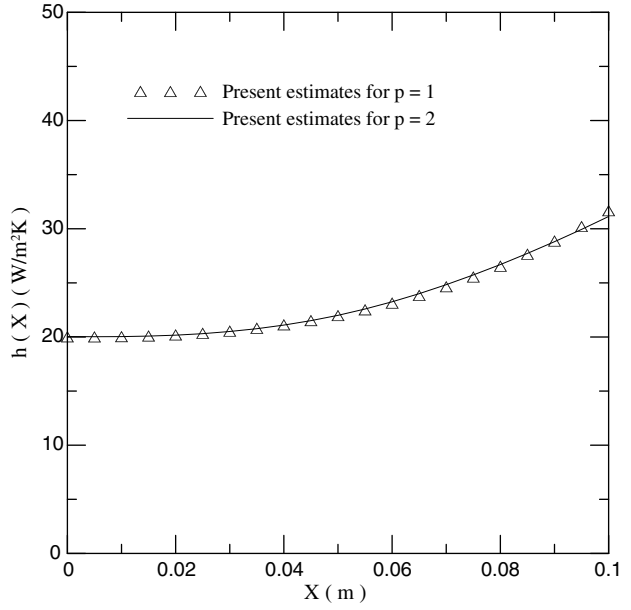

Fig. 5. Comparison of the overall heat transfer coefficient $h(X)$ for RH = 50%, $V_{air} = 0.5$ m/s and various p values.

The results show that the present estimated results for $p = 1$ and 2 show no obvious deviations. Their maximum relative error value is about 1.53%. Thus $p = 1$ is taken for all the following inverse calculations through this experimental example. Fig. 6 shows the distribution of the unknown heat-transfer coefficient $h(X)$ for various V_{air} and RH values. It can be found from Fig. 3 of Ref. [11] that there is a more droplets accumulation for RH = 90% than for RH = 50% under the same operating conditions. In addition, the wet portion on the fin is also increased with increasing the RH value. Higher RH values indicate a higher amount of mass transfer and a higher amount of latent energy. On the other hand, a larger relative humidity can cause a higher latent heat-transfer and lower fin surface temperature. Moreover, a higher air speed translates into a larger mass of moisture flowing across the fin surface under the same RH value. It can be observed from Fig. 4 of Ref. [11] that the whole fin is in partially wet condition for RH = 50% and is in fully wet condition for RH = 90% when $V_{air} = 0.5$ m/s and 4 m/s. The whole fin is in fully wet condition for $V_{air} = 0.5$ m/s and is in partially wet condition for $V_{air} = 4$ m/s under the condition of RH = 70%. This implies that a higher air speed can blow away a larger mass of the condensate on the fin under the same RH value, and the dry-wet boundary is upwardly moved with increasing the RH value. It can be observed from Fig. 3 of Ref. [11] that the droplets on the fin is not very much for RH = 50% and $V_{air} = 0.5$ m/s and 4 m/s. Under this circumstance, the effect of the droplets on the unknown overall heat-transfer coefficient h(X) cannot be significant for RH = 50% and $V_{air} = 0.5$ m/s and 4 m/s. Thus $h(X)$ can display the monotonous increase along the X-direction, as shown in Fig. 6. However, the effect of the droplets on $h(X)$ gradually becomes significant with increasing the RH value especially for $V_{air} = 0.5$ m/s. This implies that the contribution of mass transfer may be much than the sensitive heat transfer under these conditions so that $h(X)$ increases with increasing the RH value for a fixed V_{air} value. As stated by Lin et al. [11], the formation of droplet can be seen only in the vicinity of the fin base for $V_{air} = 4$ m/s and RH = 50%. The drop size at the boundary separating the dry and wet portions is very fine and increases as it approaches to the fin base. Due to the action of the gravity, the larger droplets may randomly roll down along the fin from the fin tip and may result in the random distribution of droplets on the fin due to the airflow coming into the region between two parallel fins. These droplets can accumulate in the vicinity of the fin base. It can be found from Figs. 3(b) and 3(c) of Ref. [11] that there is a more droplets

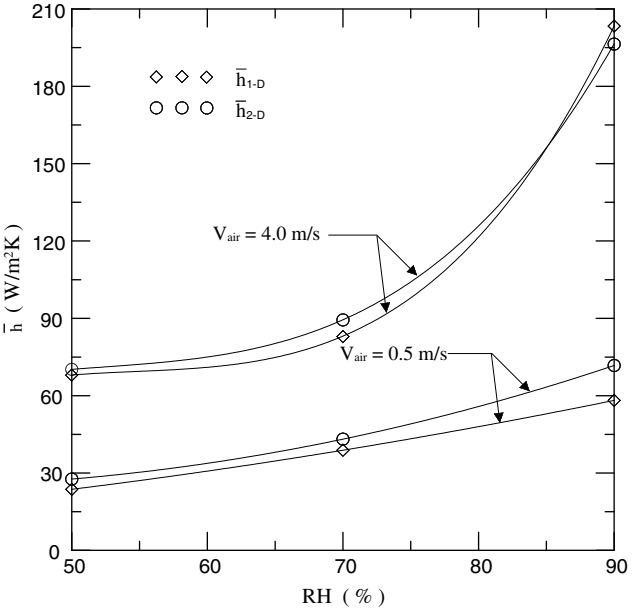

Fig. 7. Variation of the $\bar{h}$ value with the RH value for various V_{air} values.

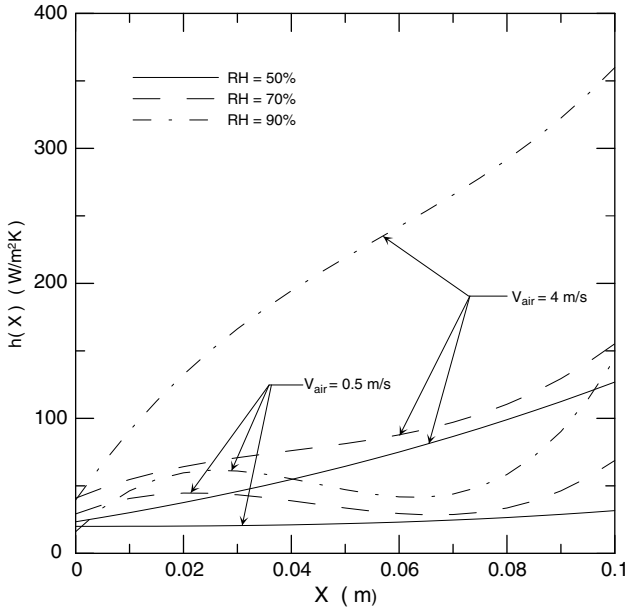

Fig. 6. Distribution of $h(X)$ for various V_{air} and RH values.

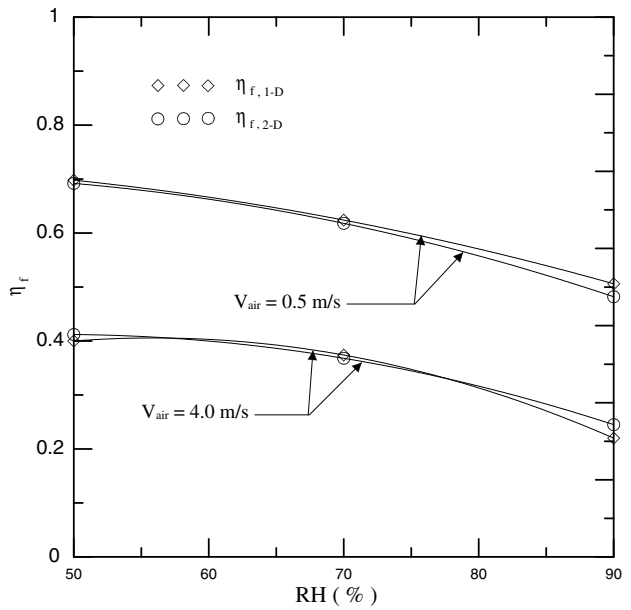

Fig. 8. Variation of the η_f value with the RH value for various V_{air} values.

accumulation in the neighborhood of the fin base and fin tip for RH = 70% and 90%. This implies that the contribution of mass transfer may be much than the sensitive heat transfer in these regions for RH = 70% and 90%. In addition, It is found from Fig. 4 of Ref. [11] that the measured fin temperatures at $Y = 0.25L$ and $X = 0.5L$, $0.6L$ and $0.7L$ exhibit $T(X = 0.6L) > T(X = 0.5L) > T(X = 0.7L)$ for RH = 70% and 90%. It is obvious that there can be a slight error in these measured results. Thus the distribution of the unknown overall heat-transfer coefficient that shows a peculiarity in nature of the wave-like distribution for $V_{air} = 0.5$ m/s and RH = 70% and 90% can result from the random distribution of droplets on the fin or the temperature measurement errors. This result can require the further validation. Fig. 6 also displays that the $h(X)$ value is increased with increasing the V_{air} value for a fixed RH value.

Figs. 7 and 8, respectively shows variation of the average overall heat transfer coefficient $\bar{h}$ and wet fin efficiency η_f obtained from the 1-D and 2-D models with the RH value for various V_{air} values. It can be observed that the $\bar{h}$ value increase with increasing the RH value for a fixed V_{air} value.

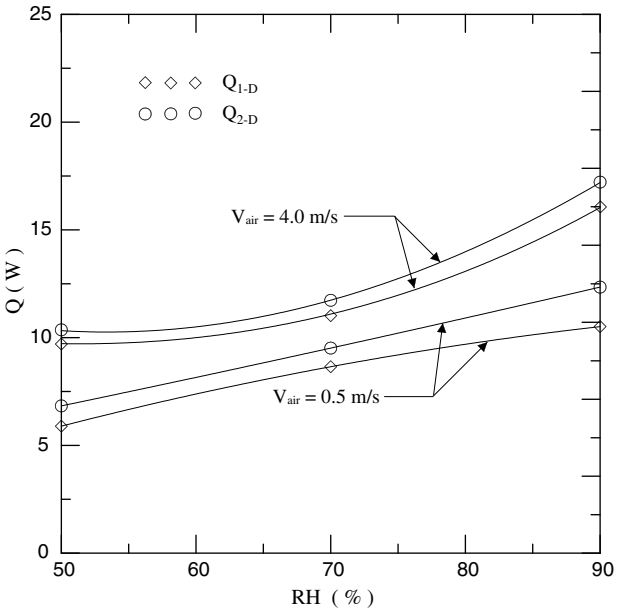

Fig. 9. Variation of the Q value with the RH value for various V_{air} values.

Table 4
Effect of the RH value on the present estimates of $\bar{h}$, Q and η_f for $p = 1$, 1-D model and various V_{air} values

	RH = 50%		RH = 70%		RH = 90%	
	$V_{air} = 0.5$ m/s	$V_{air} = 4$ m/s	$V_{air} = 0.5$ m/s	$V_{air} = 4$ m/s	$V_{air} = 0.5$ m/s	$V_{air} = 4$ m/s
$\bar{h}$ (W/m^2 K)	23.272	68.023	38.838	83.108	58.173	203.429
Q (W)	5.746	9.722	8.651	11.093	10.511	16.037
η_f	0.698	0.400	0.624	0.374	0.506	0.221

Table 5
Present estimates for the 2-D model and various V_{air} and RH values

	RH = 50%		RH = 70%		RH = 90%	
	$V_{air} = 0.5$ m/s	$V_{air} = 4$ m/s	$V_{air} = 0.5$ m/s	$V_{air} = 4$ m/s	$V_{air} = 0.5$ m/s	$V_{air} = 4$ m/s
T_j^{mea} (K)	$T_1^{mea} = 283.6$	$T_1^{mea} = 284.5$	$T_1^{mea} = 283.9$	$T_1^{mea} = 284.8$	$T_1^{mea} = 284.6$	$T_1^{mea} = 285.6$
	$T_2^{mea} = 284.3$	$T_2^{mea} = 285.3$	$T_2^{mea} = 285.1$	$T_2^{mea} = 285.6$	$T_2^{mea} = 286.2$	$T_2^{mea} = 287.3$
	$T_3^{mea} = 285.8$	$T_3^{mea} = 288.4$	$T_3^{mea} = 286.7$	$T_3^{mea} = 289.4$	$T_3^{mea} = 288.2$	$T_3^{mea} = 291.3$
	$T_4^{mea} = 287.3$	$T_4^{mea} = 290.2$	$T_4^{mea} = 289.0$	$T_4^{mea} = 291.5$	$T_4^{mea} = 290.8$	$T_4^{mea} = 294.2$
	$T_5^{mea} = 287.4$	$T_5^{mea} = 291.5$	$T_5^{mea} = 288.8$	$T_5^{mea} = 292.7$	$T_5^{mea} = 290.7$	$T_5^{mea} = 295.2$
	$T_6^{mea} = 289.0$	$T_6^{mea} = 293.4$	$T_6^{mea} = 291.3$	$T_6^{mea} = 294.5$	$T_6^{mea} = 293.4$	$T_6^{mea} = 297.4$
	$T_7^{mea} = 288.5$	$T_7^{mea} = 293.7$	$T_7^{mea} = 290.3$	$T_7^{mea} = 294.8$	$T_7^{mea} = 292.3$	$T_7^{mea} = 297.4$
	$T_8^{mea} = 290.0$	$T_8^{mea} = 295.1$	$T_8^{mea} = 292.7$	$T_8^{mea} = 296.0$	$T_8^{mea} = 294.8$	$T_8^{mea} = 298.5$
	$T_9^{mea} = 289.1$	$T_9^{mea} = 294.9$	$T_9^{mea} = 291.0$	$T_9^{mea} = 295.8$	$T_9^{mea} = 293.1$	$T_9^{mea} = 298.3$
	$T_{10}^{mea} = 290.7$	$T_{10}^{mea} = 296.2$	$T_{10}^{mea} = 293.1$	$T_{10}^{mea} = 297.0$	$T_{10}^{mea} = 295.8$	$T_{10}^{mea} = 299.1$
$\bar{h}_j$ (W/m^2 K)	$\bar{h}_1 = 19.67$	$\bar{h}_1 = 25.57$	$\bar{h}_1 = 20.90$	$\bar{h}_1 = 18.66$	$\bar{h}_1 = 44.38$	$\bar{h}_1 = 34.65$
	$\bar{h}_2 = 50.95$	$\bar{h}_2 = 50.57$	$\bar{h}_2 = 69.80$	$\bar{h}_2 = 79.36$	$\bar{h}_2 = 122.84$	$\bar{h}_2 = 188.80$
	$\bar{h}_3 = 8.85$	$\bar{h}_3 = 13.62$	$\bar{h}_3 = 6.75$	$\bar{h}_3 = 46.05$	$\bar{h}_3 = 14.47$	$\bar{h}_3 = 61.33$
	$\bar{h}_4 = 57.80$	$\bar{h}_4 = 106.10$	$\bar{h}_4 = 76.12$	$\bar{h}_4 = 110.32$	$\bar{h}_4 = 133.27$	$\bar{h}_4 = 291.11$
	$\bar{h}_5 = 6.31$	$\bar{h}_5 = 26.81$	$\bar{h}_5 = 7.76$	$\bar{h}_5 = 56.51$	$\bar{h}_5 = 12.04$	$\bar{h}_5 = 136.21$
	$\bar{h}_6 = 24.01$	$\bar{h}_6 = 123.58$	$\bar{h}_6 = 84.86$	$\bar{h}_6 = 115.71$	$\bar{h}_6 = 121.09$	$\bar{h}_6 = 320.62$
	$\bar{h}_7 = 2.41$	$\bar{h}_7 = 49.74$	$\bar{h}_7 = 6.23$	$\bar{h}_7 = 58.21$	$\bar{h}_7 = 10.35$	$\bar{h}_7 = 148.27$
	$\bar{h}_8 = 38.09$	$\bar{h}_8 = 79.12$	$\bar{h}_8 = 63.40$	$\bar{h}_8 = 126.66$	$\bar{h}_8 = 65.92$	$\bar{h}_8 = 280.63$
	$h_9 = 10.68$	$h_9 = 79.50$	$h_9 = 12.47$	$h_9 = 82.79$	$h_9 = 16.74$	$h_9 = 183.57$
	$h_{10} = 57.69$	$h_{10} = 147.47$	$h_{10} = 83.12$	$h_{10} = 200.14$	$h_{10} = 175.97$	$h_{10} = 319.86$
$\bar{h}$ (W/m^2 K)	27.65	70.21	43.14	89.44	71.71	196.51
Q (W)	6.83	10.32	9.52	11.74	12.35	17.19
η_f	0.69	0.41	0.62	0.37	0.48	0.25

The η_f value decreases with increasing the RH value. The variation of the η_f value with the RH value is similar to the works of Chen [10] and Rasario and Rahman [16]. On the other hand, the wet fin efficiency is dependent on the relative humidity. However, the work of Lin et al. [11] showed that the effect of the relative humidity on the fully wet fin efficiency is small. Thus the present results of the η_f value differ from those proposed by Lin et al. [11]. This discrepancy may result from the assumptions of the constant h_s value and the functional form between "$\omega_f - \omega_a$" and "$T - T_a$", etc. However, Lin et al. [11] did not give a complete data about the variation of the η_f value with the RH value for $T_a = 300.15$ K, $T_b = 282.15$ K, fin spacing = 0.003 m and various V_{air} values. Thus a comparison of the η_f value between the present estimates and those given by Lin et al. [11] for various RH and V_{air} values cannot be made except for the case with $V_{air} = 0.5$ m/s and RH = 70%. It is found from Fig. 5 of Ref. [11] and Tables 4 and 5 that the present estimates of the η_f value obtained from the 1-D and 2-D models about exceed that given by Lin et al. [11] about 26% for $V_{air} = 0.5$ m/s and RH = 70%.

The correlations of $\bar{h} - \mathrm{RH}$ and $\eta_f - \mathrm{RH}$ for the 1-D model can be determined using the least-square fitting method of experimental data and can be expressed as

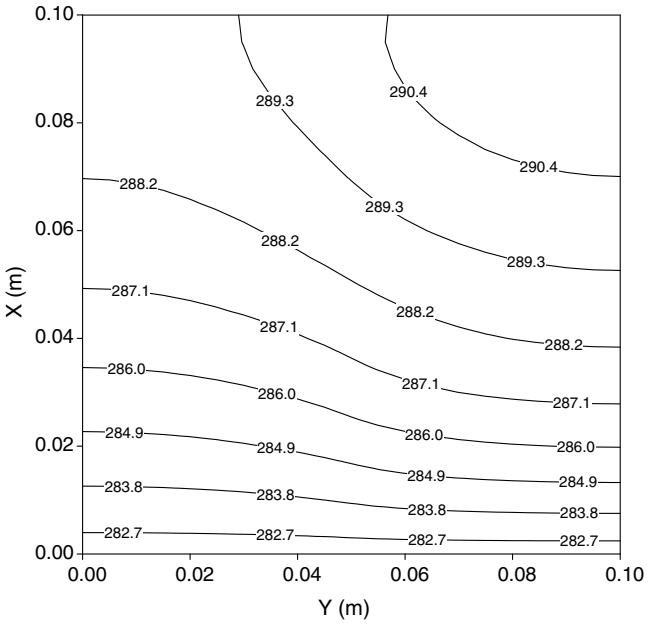

Fig. 10. Distribution of the calculated fin temperature for RH = 50% and $V_{air} = 0.5$ m/s.

$$\bar{h}_{1\text{-D}} = \begin{cases} 9.61 - 0.19 \times \mathrm{RH} + 0.01 \times \mathrm{RH}^2 - 2.78 \times 10^{-5} \times RH^3 & \text{for } V_{air} = 0.5\ \mathrm{m/s} \\ -306.15 + 21.14 \times \mathrm{RH} - 0.40 \times \mathrm{RH}^2 + 2.53 \times 10^{-3} \times \mathrm{RH}^3 & \text{for } V_{air} = 4\ \mathrm{m/s} \end{cases} \quad (49)$$

and

$$\eta_{f,1\text{-D}} = \begin{cases} 0.64 + 4.17 \times 10^{-3} \times \mathrm{RH} - 6.29 \times 10^{-5} \times \mathrm{RH}^2 & \text{for } V_{air} = 0.5\ \mathrm{m/s} \\ -5.92 \times 10^{-2} + 1.67 \times 10^{-2} \times \mathrm{RH} - 1.51 \times 10^{-4} \times \mathrm{RH}^2 & \text{for } V_{air} = 4\ \mathrm{m/s} \end{cases} \quad (50)$$

Table 4 shows that the effect of the RH value on the present estimates of the unknown average overall heat-transfer coefficient $\bar{h}$, total heat-transfer rate Q and wet fin efficiency η_f for the 1-D model and various V_{air} values. The $\bar{h}$ value in the range of $V_{air} = 0.5$–4 m/s increases from 23.272 W/m^2 K to 68.023 W/m^2 K for RH = 50% and a partially wet fin and from 58.173 W/m$^2 \cdot$ K to 203.429 W/m^2 K for RH = 90% and a fully wet fin. The $\bar{h}$ value in the range of RH = 50–90% increases from 23.272 W/m^2 K to 58.173 W/m^2 K for $V_{air} = 0.5$ m/s and from 68.023 W/m^2 K to 203.429 W/m^2 K for $V_{air} = 4$ m/s. This implies that the effect of the RH value on the $\bar{h}$ value for $V_{air} = 4$ m/s is greater than that for $V_{air} = 0.5$ m/s. The ratio of the Q value for RH = 90% to that for RH = 50% is about 1.83 times when $V_{air} = 0.5$ m/s and is about 1.65 times when $V_{air} = 4$ m/s. It is obvious that the effect of the relative humidity on the Q value for $V_{air} = 4$ m/s is less than that for $V_{air} = 0.5$ m/s. The η_f value in the range of $V_{air} = 0.5$–4 m/s decreases from 0.698 to 0.4 for RH = 50% and a partially wet fin and from 0.506 to 0.221 for RH = 90% and a fully wet fin. This result implies that the effect of the RH value on the η_f value for $V_{air} = 4$ m/s is greater than that for $V_{air} = 0.5$ m/s because a higher air speed can blow away a larger mass of the condensate on the fin. The above results show that the larger the V_{air} value is, the greater the effect of the relative humidity on the $\bar{h}$ and η_f values can be.

The curve-fitted fin temperatures $T_1^{mea}, T_2^{mea}, \ldots, T_{10}^{mea}$ are shown in Table 5 for $T_a = 300.15$ K, $T_b = 282.15$ K and value V_{air} and RH. Table 5 also shows the effect of the RH value on the average overall heat-transfer coefficient on the jth sub-fin region $\bar{h}_j$, total heat-transfer rate Q, average overall heat-transfer coefficient on the fin $\bar{h}$ and wet fin efficiency η_f. It can found from Ref. [4] that the flow structure for the airflow coming into the region between two parallel fins was complex under dry conditions due to the free-stream interaction, fluid separation and reattachment, etc. The dynamics of flow and sensitive heat transfer are strongly three-dimensional and the average convective heat transfer coefficient is closely related to the fin spacing and Reynolds number. A low-velocity

region can occur in the downstream sub-fin regions. It can be found from Table 5 that the fin temperatures in the downstream fin region are higher than those in the upstream fin region. However, the temperature difference between the fin temperature and air ambient temperature in the upstream region is higher than that in the downstream for the present problem. Rosario and Rahman [16] stated that the sensible heat transfer is due to convection from the air to the fin because of the temperature difference between the fin temperature and air ambient temperature. Lin et al. [11] also stated that the dry portion near the leading edge was larger than that in the downstream fin region or the trailing region. On the other hand, a greater droplet accumulation can occur in the downstream fin region. This implies that the contribution of the latent heat transfer due to mass transfer may be more than the sensitive heat transfer in the downstream fin region. Thus the overall heat-transfer coefficients in the downstream sub-fin regions may be greater than those in the upstream sub-fin regions under wet conditions, as shown in Table 5. It is known that the 2-D model can take into account the variation of the heat-transfer characteristics on the fin. On the other hand, the 2-D model can provide insight of the flow and heat-transfer characteristics that are difficult to be revealed by using the 1-D model. Therefore, in order to enhance the overall heat transfer, it is worth to find a way to increase heat transfer in the upstream fin regions for the present problems. This may lead to design a heat exchanger with a high heat transfer performance under wet conditions. As stated by Rosario and Rahman [16], the latent heat transfer due to condensation was a very significant portion of the total heat transfer and should not be ignored in any aspect of the

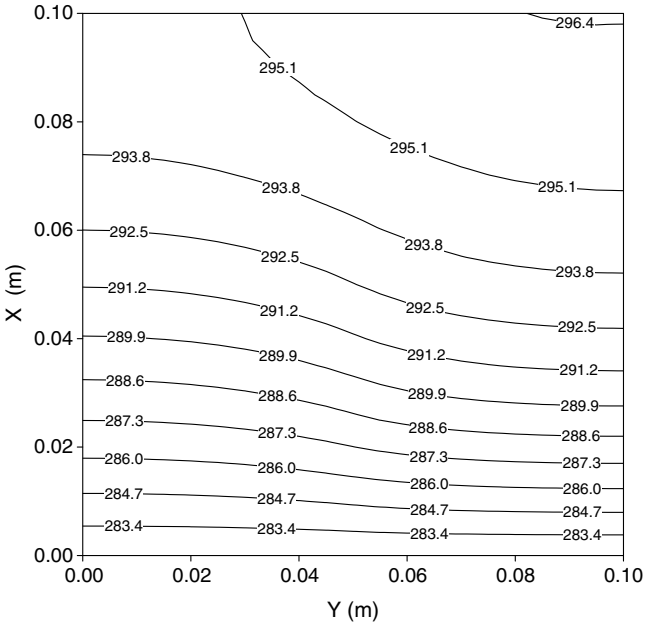

Fig. 11. Distribution of the calculated fin temperature for RH = 50% and $V_{air} = 4.0$ m/s.

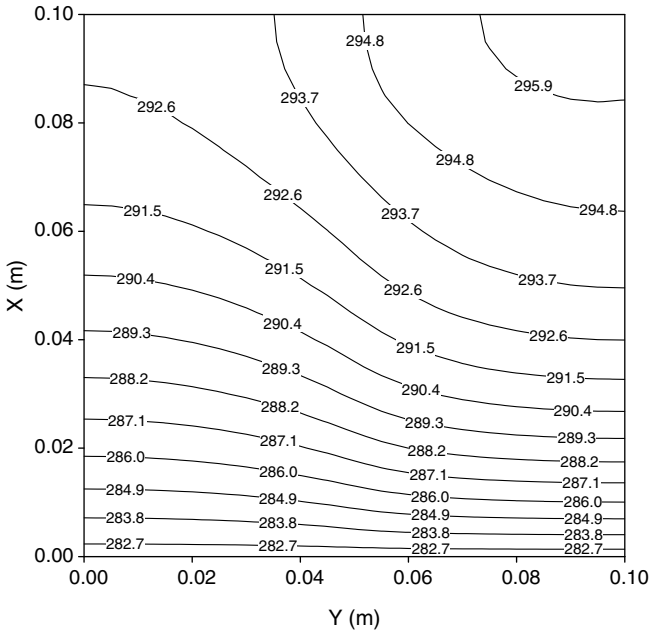

Fig. 12. Distribution of the calculated fin temperature for RH = 90% and $V_{air} = 0.5$ m/s.

dehumidification design. Thus the estimation of the average overall heat-transfer coefficient on each sub-fin region is an important task for the present problem.

The numerical results of Liang et al. [3] showed that the η_f values obtained from the 1-D model compared well with those obtained from the 2-D model for various RH values. However, It is observed from Tables 4 and 5 that the present estimates of the η_f value agree with those obtained from the 1-D model for RH $\leqq$ 70% and slightly deviate from those obtained from the 1-D model for RH >70% when $V_{air} = 0.5$ m/s and 4 m/s. The $\bar{h}$ and Q values obtained from the 2-D model also deviate from those obtained from the 1-D model for various V_{air} and RH values. The maximum deviations of the $\bar{h}$, Q and η_f values for the 1-D and 2-D models, respectively are about 18.9%, 14.9% and 11.6%. This discrepancy can result from the variation of the overall heat-transfer coefficient on the fin. As stated by Liang et al. [3], the function of the overall heat-transfer coefficient on the fin can be incorporated into the 2-D model to further improve the model accuracy. The effect of the RH value on the $\bar{h}$ value was not discussed in the work of Liang et al. [3].

Fig. 9 shows variation of the total heat-transfer rate Q obtained from the 1-D and 2-D models with the RH value for various V_{air} values. It can be observed that the Q value increases with increasing the RH value for a fixed V_{air} value. The estimated values of the total heat-transfer rate Q using the 2-D model are larger than those using the 1-D model. Their discrepancy can become large with increasing the RH value.

The smoothing curves can be applied to match the data points of $\bar{h} - \mathrm{RH}$ and $\eta_f - \mathrm{RH}$. The correlations of $\bar{h} - \mathrm{RH}$ and $\eta_f - \mathrm{RH}$ obtained from the 2-D model can be deter-

mined using the least-square fitting method of experimental data and can be expressed as

$$\bar{h}_{2\text{-D}} = \begin{cases} 73.39 - 2.43 \times \mathrm{RH} + 3.45 \times 10^{-2} \times \mathrm{RH}^2 - 8.66 \times 10^{-5} \times \mathrm{RH}^3 & \text{for } V_{\mathrm{air}} = 0.5\ \mathrm{m/s} \\ 75.14 + 2.83 \times \mathrm{RH} - 0.11 \times \mathrm{RH}^2 + 1.05 \times 10^{-3} \times \mathrm{RH}^3 & \text{for } V_{\mathrm{air}} = 4\ \mathrm{m/s} \end{cases} \tag{51}$$

and

$$\eta_{\mathrm{f,2\text{-D}}} = \begin{cases} 0.605 + 5.6 \times 10^{-3} \times \mathrm{RH} - 7.55 \times 10^{-5} \times \mathrm{RH}^2 & \text{for } V_{\mathrm{air}} = 0.5\ \mathrm{m/s} \\ 0.18 + 9.65 \times 10^{-3} \times \mathrm{RH} - 9.88 \times 10^{-5} \times \mathrm{RH}^2 & \text{for } V_{\mathrm{air}} = 4\ \mathrm{m/s} \end{cases} \tag{52}$$

Once the average overall heat-transfer coefficient on each sub-fin region is obtained, the temperature distribution in the fin can also be determined from the similar matrix equation shown in Eq. (26). However, it should be noted that the average overall heat-transfer coefficient on each sub-fin region is an approximate value. Thus the temperature distribution in the fin is also an approximate contour for various $\varepsilon\sigma$ and RH values. Figs. 10 and 11, respectively show the distributions of the calculated fin temperature for RH = 50% and $V_{\mathrm{air}} = 0.5$ m/s and 4 m/s. The distributions of the calculated fin temperature for RH = 90% and $V_{\mathrm{air}} = 0.5$ m/s and 4 m/s are respectively shown in Figs. 12 and 13. It can be observed from Figs. 10–13 that there is a considerable temperature drop between the fin base and the fin tip in the downstream region because the more amount of droplets accumulated on this region. The fin temperature increases more rapidly away from the fin base with increasing the V_{air} and RH values.

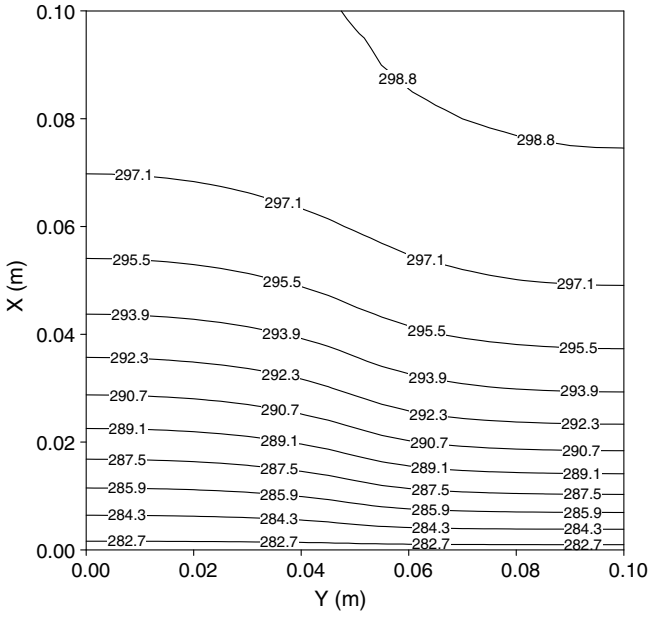

Fig. 13. Distribution of the calculated fin temperature for RH = 90% and $V_{\mathrm{air}} = 4.0$ m/s.

5. Conclusions

The present study proposes the 1-D and 2-D inverse heat conduction schemes involving the finite difference method in conjunction with the least-squares method and measured fin temperatures at various measurement locations to estimate the unknown average overall heat-transfer coefficient on the fin $\bar{h}$, total heat-transfer rate Q and wet fin efficiency η_{f} for various V_{air} and RH values. The results show that the present estimates of the η_{f} value decrease with increasing the RH value. On the other hand, the wet fin efficiency under partially and fully wet conditions is sensitive to the relative humidity. The interesting findings are that the present estimates of the η_{f} value using the 2-D model agree with those using the 1-D model for RH $\leqq$ 70% and slightly deviate from those obtained from the 1-D model for RH $>$ 70% at $V_{\mathrm{air}} = 0.5$ m/s and 4 m/s. The present estimates of the $\bar{h}$ and Q values using the 2-D model slightly deviate from those using the 1-D model for various V_{air} and RH values. The maximum deviations of the $\bar{h}$, Q and η_{f} values for the 1-D and 2-D models, respectively are about 18.9%, 14.9% and 11.6%. It is worth noting that the average overall heat-transfer coefficient in the downstream region may be larger than that in the upstream region under wet conditions. Thus the latent heat transfer under wet conditions is a very significant portion of the total heat transfer and should not be negligent in any aspect of the dehumidification design.

References

[1] B. Kundu, Performance and optimum design analysis of longitudinal and pin fins with simultaneous heat and mass transfer: unified and comparative investigations, Appl. Thermal Eng. 27 (2007) 976–987.
[2] C.N. Lin, J.Y. Jang, A two-dimensional fin efficiency analysis of combined heat and mass transfer in elliptic fins, Int. J. Heat Mass Transfer 45 (2002) 3839–3847.
[3] S.Y. Liang, T.N. Wong, G.K. Nathan, Comparison of one-dimensional and two-dimensional models for wet-surface fin efficiency of a plate-fin-tube heat exchanger, Appl. Thermal Eng. 20 (2000) 941–962.
[4] E. Velayati, M. Yaghoubi, Numerical study of convective heat transfer from an array of parallel bluff plates, Int. J. Heat Fluid Flow 26 (2005) 80–91.

[5] F.E.M. Saboya, E.M. Sparrow, Local and average heat transfer coefficients for one-row plate fin and tube heat exchanger configurations, ASME J. Heat Transfer 96 (1974) 265–272.
[6] H.T. Chen, J.P. Song, Y.T. Wang, Prediction of heat transfer coefficient on the fin inside one-tube plate finned-tube heat exchangers, Int. J. Heat Mass Transfer 48 (2005) 2697–2707.
[7] H.T. Chen, J.C. Chou, Investigation of natural-convection heat transfer coefficient form the vertical fin of finned-tube heat exchangers, Int. J. Heat Mass Transfer 49 (2006) 3034–3044.
[8] H.T. Chen, J.C. Chou, Estimation of heat transfer coefficient on the vertical plate fin of finned-tube heat exchangers for various air speeds and fin spacings, Int. J. Heat Mass Transfer 50 (2007) 45–57.
[9] H.T. Chen, W.L. Hsu, Estimation of heat transfer coefficient on the fin of annular-finned tube heat exchangers in natural convection for various fin spacings, Int. J. Heat Mass Transfer 50 (2007) 1750–1761.
[10] L.T. Chen, Two-dimensional fin efficiency with combined heat and mass transfer between water-wetted fin surface and moving moist airstream, Int. J. Heat Fluid Flow 12 (1991) 71–76.
[11] Y.T. Lin, K.C. Hsu, Y.J. Chang, C.C. Wang, Performance of rectangular fin in wet conditions: visualization and wet fin eifficiency, ASME J. Heat Transfer 123 (2001) 827–836.
[12] R.L. Webb, Principles of Enhanced Heat Transfer, Wiley, New York, 1994, pp. 125–153.
[13] A.H. Elmahdy, R.C. Biggs, Efficiency of extended surfaces with simultaneous heat transfer and mass transfer, ASHRAE J. 89 (1A) (1983) 135–143.
[14] J.E.R. Coney, C.G.W. Sheppard, E.A.M. El-Shafei, Fin performance with condensation from humid air, Int. J. Heat Fluid Flow 10 (1989) 224–231.
[15] F.C. McQuiston, Fin efficiency with combined heat and mass transfer, ASHRAE J. 81 (1975) 350–355.
[16] L. Rosario, M.M. Rahman, Analysis of heat transfer in a partially wet radial fin assembly during dehumidification, Int. J. Heat Fluid Flow 20 (1999) 642–648.
[17] J.L. Threlkeld, Thermal Environmental Engineering, second ed., Prentice-Hall, Englewood Cliffs, New Jersey, 1970.
[18] ARI Standard 410-91, Forced-circulation air-cooling and air-heating coils, Air-Conditioning & Refrigeration Institute, Arlingtion, 1991.
[19] C.D. Ware, T.H. Hacha, Heat transfer form humid air to fin and tube extended surface cooling coils, ASME paper 60-HT-17 1960.
[20] M.N. Özisik, Heat Conduction, second ed., Wiley, New York, 1993.
[21] K. Kurpisz, A.J. Nowak, Inverse Thermal Problems, Computational Mechanics Publications, Southampton, UK, 1995.
[22] G.D. Raithby, K.G.T. Hollands, Natural convection, in: W.M. Rohsenow, J.P. Hartnett, E.N. Ganic (Eds.), Handbook of Heat Transfer Fundamentals, second ed., McGraw-Hill, New York, 1985.
[23] F. Kreith, M.S. Bohn, Principles of Heat Transfer, fifth ed., Springer, New York, 1993.
[24] T.H. Chilton, A.P. Colburn, Mass transfer coefficient, Int. Eng. Chem. 26 (1934) 1183–1187.
[25] A. Bejan, Heat Transfer, John Wiley & Sons Inc., New York, 1993.
[26] H.T. Chen, X.Y. Wu, Estimation of heat transfer coefficient in two-dimensional inverse heat conduction problems, Numer. Heat Transfer B 50 (2006) 375–394.
[27] H.T. Chen, X.Y. Wu, Estimation of surface conditions for nonlinear inverse heat conduction problems using the hybrid inverse scheme, Numer. Heat Transfer B 51 (2007) 159–178.
[28] H.T. Chen, Y.X. Wu, Estimation of surface absorbtivity in laser surface heating process with experimental data, J. Phys. D: Appl. Phys. 39 (2006) 1141–1148.
[29] J.P. Holman, Experimental Methods for Engineers, McGraw-Hill, New York, 2001.
[30] ASHARE Standard 33-78, Method of testing forced circulation air cooling and air heating coils, American Society of Heating Refrigerating and Air-conditioning Engineers, Inc., Atlanta, 1978.
[31] ASHARE Standard 41.2-1987, Standard method for laboratory airflow measurement, American Society of Heating Refrigerating and Air-conditioning Engineers, Inc., Atlanta, 1987.
[32] ASHARE Standard 41.1-1986, Standard method for temperature measurement, American Society of Heating Refrigerating and Air-conditioning Engineers, Inc., Atlanta, 1986.